The double-ITCZ syndrome in coupled general circulation models: the role of large-scale vertical circulation regimes.

A. Bellucci[1], S. Gualdi[1,2], and A. Navarra[1,2]

[1]Centro Euro-Mediterraneo per i Cambiamenti Climatici, Bologna, Italy
[2]Istituto Nazionale di Geofisica e Vulcanologia, Bologna, Italy

Manuscript submitted to

Journal of Climate

August 14, 2009

[0]*Correspondence to:* A. Bellucci
Centro Euro-Mediterraneo per i Cambiamenti Climatici
Viale A. Moro 44
I-40127 Bologna, Italy
e-mail bellucci@bo.ingv.it
Phone +39 051 3782609
Fax +39 051 3782655

Abstract

The double-intertropical convergence zone (DI) systematic error, affecting state-of-the-art coupled general circulation models (CGCM) is examined in the multi-model Intergovernmental Panel on Climate Change (IPCC) Fourth Assessment Report (AR4) ensemble of simulations of the twentieth-century climate. Aim of this study is to quantify the DI error on precipitation in the tropical Pacific, with a specific focus on the relationship between the DI error and the representation of large-scale vertical circulation regimes in climate models. The DI rainfall signal is analysed using a regime sorting approach for the vertical circulation regimes. Through the use of this compositing technique, precipitation events are regime-sorted based on the large scale vertical motions, as represented by the mid-tropospheric lagrangian pressure tendency ω_{500} dynamical proxy. This methodology allows the partition of the precipitation signal into deep and shallow convective components. Following the regime-sorting diagnosis, the total DI bias is split into an error affecting the magnitude of precipitation associated with individual convective events and an error affecting the frequency of occurrence of single convective regimes. It is shown that, despite the existing large intra-model differences, CGCMs can be ultimately grouped into a few homegenous clusters, each featuring a well defined rainfall-vertical circulation relationship in the DI region. Three major behavioural clusters are identified within the AR4 models ensemble: two unimodal distributions, featuring maximum precipitation under subsidence and deep convection regimes, respectively, and one bimodal distribution, displaying both components. Extending this analysis to both coupled and uncoupled (atmosphere-only) AR4 simulations reveals that the DI bias in CGCMs is mainly due to the overly frequent occurrence

of deep convection regimes, whereas the error on rainfall magnitude associated with individual convective events is overall consistent with errors already present in the corresponding atmosphere stand-alone simulations. A critical parameter controlling the strength of the DI systematic error is identified in the model-dependent sea surface temperature (SST) threshold leading to the onset of deep convection (THR), combined with the average SST in the south-eastern Pacific. The models featuring a THR which is systematically colder (warmer) than their mean surface temperature are more (less) prone to exhibit a spurious southern Intertropical Convergence Zone.

1 Introduction

The intertropical convergence zone (ITCZ) is a zonally elongated narrow band of enhanced low-level wind convergence, cloudiness and rainfall, marking the upward branch of the Hadley circulation cell. A fascinating feature displayed by the ITCZ over the Pacific and Atlantic oceans is the off-equatorial preference location, in the northern hemispheric 4-12^o latitude belt. The existence of one single ITCZ straddling the Northern Hemisphere has been puzzling theoreticians for quite a long time, trying to understand the causes of such an asymmetric response to the essentially symmetric solar radiation forcing (Charney,1971; Holton et al.,1971; Waliser and Somerville, 1994; Philander et al., 1996). Idealized experiments performed with aqua-planet model settings forced by highly symmetric SST distributions show no unequivocal responses, with either two off-equatorial ITCZs (Hayashi and Sumi 1986; Swinbank et al. 1988) or one single ITCZ centered on the equator, coincident with the maximum SST location (Lau et al. 1988). Hess et al. (1993) using similar aqua-planet model configurations, identify a strong dependency of ITCZ location on the adopted parametrization for convection and the strength of the SST meridional gradient. The vast majority of coupled general circulation models (CGCM) show the occurrence of an overly strong ITCZ in the south-eastern Pacific region, in a broad region off Peru near 10^{o}S (Mechoso et al., 1995). While the appearence of a southern hemispheric ITCZ in March-April is an observed feature of the tropical Pacific climate, its overestimation represents a well known *syndrome* affecting state-of-the-art climate models which is generally referred to as double-ITCZ (here after DI; Mechoso et al., 1995). This bias affects climate models ability in correctly reproducing some of the most prominent climatological features of the tropical Pacific. In particular, the representation of the mean state in the Pacific sector displays an anomalous symmetric structure about the equator contrasting with the asymmetry characterising the observed annual mean patterns of rainfall, sea surface temperature and wind, possibly reflecting the interhemispheric differences for the oceans and continents distribution (Philander et al. 1996; Ma et al.,1996; Yu and Mechoso, 1999). DIs in CGCMs are generally associated with a an anomalously extended

cold tongue on the equator (a quite distinctive feature with respect to aqua-planet configurations) and they typically manifest themselves with a wide spectrum of behaviours (Mechoso et al. 1995; Lin, 2007). De Szoeke and Xie (2008) classify the error associated with ITCZ representation in AR4 models according to the mean seasonal evolution of precipitation, identifying two distinct error typologies: *persistent double ITCZ* error (rain persisting too long in the Southern Hemisphere) and *alternating ITCZ* error (precipitation maxima crossing the equator with the season). Both of them lead to a spuriously high annual mean precipitation in the south-eastern tropical Pacific.

Since the early assessment of Mechoso et al. (1995), the overall performance of climate models has been gradually improving through the years (Meehl 2005). However, the erroneous representation of the tropical climate remains a severe limitation for the current generation of CGCMs, recently employed to perform climate projections within the Intergovernmental Panel on Climate Change Fourth Assessment Report effort (IPCC AR4; Lin, 2007; de Szoeke and Xie, 2008), ultimately impacting on the predictability and simulation of tropical variability modes (El Niño-Southern Oscillation, Madden-Julian Oscillation) on seasonal and interannual time scales. The availability of AR4 experiments archived by the Program for Climate Model Diagnosis and Intercomparison (PCMDI) allows the cross-comparison of an ensemble of CGCMs, combining different parameterizations of unresolved physics as well as spatial resolutions and numerical schemes. Recently, the DI issue (and, more broadly, the models systematic errors in the tropical eastern pacific) in AR4 simulations of the twentieth century climate has been examined under different perspectives. Lin (2007) approaches the DI bias in relation with the representation of the main ocean-atmosphere feedbacks, whereas de Szoeke and Xie (2008) focus on the role played by the meridional wind biases in relationship with the interaction with the complex Central American orography.

The purpose of this study is to analyse the relationships between the bias on precipitation in the south-eastern tropical Pacific and the systematic errors affecting the underlying large-scale atmospheric vertical circulation regimes in the IPCC AR4 CGCMs. Large-

scale vertical motions in the atmosphere are responsible for heat and moisture transport, and thus play a crucial role on determining atmospheric stability, cloudiness and precipitation.

Specifically, the following issues are addressed. What is the partition of the spurious DI rainfall signal between shallow and deep convective components? Unraveling the deep from the shallow convection precipitation is a fundamental step to further disclose the nature of DI in climate models. Another crucial question concerning the DI bias is whether the detected rainfall anomaly in the south-eastern Pacific is caused by an overly frequent (either deep or shallow) convective activity or by anomalously strong precipitation associated with individual convective events. To this aim, a useful approach is provided by a composite methodology first proposed by Bony et al.(2004) for cloud feedback studies, generally referred to as regime sorting, which will be here applied to study the model-dependent relationships between precipitation and vertical circulation regimes in the region affected by the DI systematic error. Exploring a geophysical quantity in the space defined by another variable as an alternative to the standard analysis in the time-space domain allows a better identification of the physical mechanisms relating the two fields under exam. An additional advantage deriving from the use of such methodology is the identification of thresholds in the physical space defined by the two selected variables. Specifically, this approach is here extended to the SST-vertical circulation physical space so as to identify critical SSTs setting the transition to deep convection for each member of the AR4 ensemble. The interplay between errors on the SST-deep convection coupling and the biases on SST will also be investigated. The present analysis will particularly focus on the south-eastern tropical Pacific region, where the DI systematic error manifests itself.

We address these questions for both coupled and, where available, the corresponding uncoupled (i.e., AMIP-type) AR4 simulations of the twentieth century climate. The cross-comparison between coupled and AMIP simulations will provide some insight on the role played by ocean-atmosphere coupling, as compared to atmospheric internal dynamics, in

modifying the relationship between the DI spurious precipitation signal and the underlying vertical circulation regimes.

The paper is structured as follows. In section 2, the model and observational data used in this analysis are described. The space-time structure of the systematic errors affecting precipitation and vertical circulation in the tropical eastern Pacific is described in section 3. Results from the regime sorting analyis applied to the AR4 coupled simulations of the twentieth century are shown in section 4. In section 5 the same analysis is extended to a smaller set of AMIP simulations. The role of biases affecting the representation of SST and the critical SST leading to convection on the amplitude and structure of DI is investigated in section 6. Summary and conclusions are given in section 7.

2 AR4 models and validation data.

The analyses shown in the present work are based on monthly outputs from a subset of 20 AR4 CGCMs (except for the mean seasonal cycle of precipitation, where a larger 23 members ensemble is used instead). Also, a smaller set of 13 twin simulations conducted with the atmospheric-only component of the corresponding coupled models, under prescribed SSTs (AMIP-type), is analysed. The models employed in this study are listed in Table 1.

This study focuses on the IPCC Climate of the Twentieth Century (20C3M) simulation, for the 1960-2000 period. Model results are compared with both observational datasets and reanalyses (for simplicity, in the paper we will refer to both types of data as "observations"). In particular, the observed global CMAP dataset (Xie and Arkin, 1997) is used for precipitation, while for ω fields the European Centre for Medium-Range Weather Forecasts (ECMWF) ERA-40 Re-Analysis (Uppala et al., 2005) has been used. Finally, the global HadISST analyses (Rayner et al.,2003) were used for sea surface temperatures.

3 Mean seasonal cycle

In Fig. 1 the mean seasonal cycle of precipitation over the eastern Pacific (averaged between 150W and 100W) is plotted against latitude for observations (Xie and Arkin, 1997) and AR4 models. This diagnostic essentially updates the evaluation made by Mechoso et al. (1995; see also de Szoeke and Xie, 2008), and portrays the current status of CGCMs, as far as the DI bias is concerned. Assessing the occurrence of DI in models can be quite subjective, in that observations do show a hint of DI, manifesting itself as a weakening of the Northern Hemisphere ITCZ and the concomitant appearence of a southern ITCZ, from about February to April (Zhang, 2001). Following Mechoso et al. (1995), in Fig. 1 we highlight precipitation in excess of 6 mm/day which is set as an arbitrary threshold so that models overcoming this critical value south of the equator are considered to be affected by the DI bias (a more objective metric of precipitation in the south-eastern Pacific is defined below). An immediate outcome is that, except for flux adjusted models and one non-adjusted model, all of the analysed CGCMs display a spurious precipitation signal south of the equator (around 10S) mostly affecting boreal late winter/early spring period. In order to quantify the DI bias for each coupled model in a more objective way, we introduce a *southern ITCZ* (SI) index which is simply defined as the annual mean precipitation over the [100W-150W; 20S-0] longitude-latitude window. The selected spatial domain is chosen so as to account for the large intra-model spread of the bias structure. In particular, the latitude extent of the box is sufficiently wide to account for the differing DI meridional locations in the various models. While this index reflects the integral behaviour of a model over a region of the south-eastern Pacific, from Fig. 1 it is legitimate to assume that the resulting index values are mainly affected by the presence of the DI. In Fig. 2 the SI index for each member of the extended (23 members) AR4 ensemble and observations is shown. It is evident that among the models displaying a smaller discrepancy with observations are those models which make use of flux adjustments on both heat and water (CCCMA-T47, CCCMA-T63, MRI, MIUB). On the opposite side mainly appear models showing a persistent DI through most of the annual cycle (CNRM, NCAR PCM1,

INMCM3, GISS-EH). This index provides a tool to rank the AR4 CGCMs based on the models' performance in the DI region, and it will be used in the final discussion.

The nature of the spurious precipitation signal in the eastern Pacific is now analysed by looking at the mean seasonal cycle of the large scale vertical circulation. We use the lagrangian pressure tendency ω at 500 hPa (in hPa/day; hereafter ω_{500}) as a proxy of the large-scale vertical circulation. Positive values of ω_{500} identify regions of large-scale subsidence, while negative values of ω_{500} indicate regions characterised by convective regimes.

The mean seasonal cycle of ω_{500} in the [100W-150W; 20S-0] longitude-latitude range is shown in Fig. 3. The persistently positive values shown by observations (from ERA-40 reanalysis) indicate that this region of the eastern Pacific is characterised by a predominant subsidence regime (see comments in the next section). The bulk of AR4 models, on the other hand, reveals a seasonal inversion of the large scale circulation regime, with rising ($\omega_{500} < 0$) from January to May-June and sinking ($\omega_{500} > 0$) during the rest of the year. Some of the models reveal an almost persistent convective regime (NCAR PCM1 and INMCM3). A few notable exceptions are represented by HadCM3, HadGEM1 and MRI models, displaying constantly positive ω_{500} values, consistent with the observations (although the latter is a flux corrected model). The relationship between mean precipitation and ω_{500} in the DI region during JFMAMJ and JASOND is illustrated in Fig. 4. Models which are prone to display a pronounced DI bias, associated with anomalously high rainfall, are generally characterised by a consistently large ascent signal (i.e.,negative ω_{500} values). The largest model-observation discrepancies as well as inter-model scatter are found in JFMAMJ, while inter-model correlations between precipitation and ω_{500} are 0.79 and 0.85 for JFMAMJ and JASOND, respectively.

4 Regime sorting analysis

In the previous section it has been shown that the occurrence of a DI in CGCMs is generally associated with mid-troposheric large-scale rising motion ($\omega_{500} < 0$) . However,

spatial averages do not allow a clear inspection on the dynamical causes underlying the process under exam. In particular, it is unclear what is the relative role played by deep versus shallow convection in driving the anomalous precipitation associated with the DI. In order to better clarify this point we apply to each AR4 model a compositing methodology (illustrated in Bony et al., 2004), where precipitation events are regime-sorted based on the large scale vertical circulation regime (as represented by the ω_{500} dynamical proxy). This procedure is applied to monthly outputs of ω_{500} , split into bins of 10 hPa/day width (see Hourdin et al., 2006 for further details) in the [100W-150W, 20S-0] region. Before applying the regime sorted analysis, the probability density function (PDF) of the ω_{500} for models and observations is computed (Fig. 5). The PDF provides the normalised frequency of occurrence for a given regime, and it must be considered as a relative weight for the regime sorted precipitation. Observations show a marked peak around 20 hPa/day, with a sharp decline for larger ω_{500} values, and a smoother tail of negative values. This distribution essentially reflects the dominance of subsidence regimes in the tropics, which is in turn determined by the clear-sky radiative cooling characterising this particular region (Chéruy and Chevallier, 2000; Bony et al. 2004). All of the AR4 models largely agree with the observed PDF. However the frequency of occurrence of moderate-to-intense convective events ($\omega_{500} < -20$ hPa/day) is generally overestimated in the models, while the opposite tendency is exhibited in the $-10 < \omega_{500} < 10$ hPa/day range and for subsidence rates larger than 40 hPa/day. Regimes around the PDF peak (20-30 hPa/day), on the other hand, occur with a typically higher frequency compared to the observations.

The distribution of precipitation in the [100W-150W, 20S-0] region, regime sorted as a function of ω_{500} is shown in Fig. 6. The dynamical link between large scale circulation and precipitation manifests itself with the largest rainfall events occurring in concomitance with deep convective regimes, contrasted by the relatively weaker precipitation signals associated with moderate and shallow convection. Moreover, under mid-tropospheric subsidence regimes precipitation appears to be weakly dependent on the strength of sinking motion.

The comparison with observations reveals two important aspects regarding the general behaviour of AR4 models. First, none of the model precipitation curves falls below the observed distribution, regardless of the specific dynamical regime, indicating a systematic model rainfall overestimate for a given vertical circulation regime . Secondly, model-observation discrepancies are generally low for shallow convection regimes, but gradually increase with -ω_{500}, under deep convection conditions.

An aspect which is worth to examine is the relative contribution to the precipitation bias, deriving from ω_{500} PDF and the regime-sorted precipitation, as measured by $\frac{\Delta\omega}{\omega}$ and $\frac{\Delta Pr}{Pr}$, respectively, with $\Delta\omega$ (ΔPr) the pointwise difference between model and observed ω_{500} PDF (regime sorted precipitation). In the negative ω_{500} axis, where the largest precipitation events occur, $\frac{\Delta\omega}{\omega}$ reaches peaks of as much as 6, while $\frac{\Delta Pr}{Pr}$ remains confined below 1. In other words, it is the spuriously large frequency of occurrence of deep convection regimes to set the intensity of the bias, rather than the amount of precipitation that falls for a given vertical velocity.

In order to obtain a more quantitative estimate of precipitation for different vertical circulation regimes, the regime sorted values of precipitation need to be weighted by the frequency of occurrence of each ω_{500} regime interval. After combining the regime sorted precipitation with the corresponding ω_{500} PDF , we obtain the distributions shown in Fig. 7. Observations show that the largest contribution to precipitation in the area under exam clearly derives from shallow convective processes, the maximum signal occurring for ω_{500} values around 10-20 hPa/day, while moderate and intense deep convective events play a relatively minor role. The ensemble of AR4 models, on the other hand, displays a much wider range of behaviours. Based on the specific shape of the regime-weighted distributions, models can be gathered into three distinct clusters (shown in Fig. 8). A first group, identified as SUB, collects models displaying the ability of capturing the dominance of precipitation under subsidence regimes with a maximum around 20 hPa/day, consistent with the observed pattern. A second group, identified as INT, gathers models which exhibit a maximum contribution to precipitation in the deep convection regimes of moderate

intensity, with a broad intra-model peak in the (-30,-10) hPa/day range. Finally, a third cluster, labelled as HYBRID, can be identified, which collects models displaying two relative maxima, for both deep and shallow convection regimes, thus mixing together the features of SUB and INT groups.

We now evaluate the error associated with the regime sorted precipitation for each single AR4 ensemble member as the model-observation root-mean-square error (RMSE) over the (-100,+80) hPa/day ω_{500} range, and compare the resulting estimates for each cluster (Fig. 9). From the comparison, it turns out that models referring to the SUB group, except for one single outlier (the GISS-ER model; see comments below) show a RMSE which is on average lower than the average error as estimated for INT and HYBRID clusters. This indicates that models which qualitatively capture the observed rainfall pattern in the regime sorted space (SUB cluster) largely minimize the associated error on precipitation. On the other hand, the presence of spurious precipitation under deep convection regimes, particularly for intermediate strengths of convective motions, contributes to a systematically larger model error.

While the adopted approach proves to be generally skillful in segregating models which capture the dominant subsidence regime of the south-eastern Pacific (low error on precipitation) from those showing a spuriously high occurrence of deep convection (large error on precipitation) there is one notable exception, represented by the GISS-ER model. This model, despite qualitatively capturing the correct regime-sorted rainfall distribution, features an overly strong precipitation signal under subsidence conditions, which leads to a consistently high RMSE (Fig. 9). In order to further clarify this anomalous behaviour the regime-sorted analysis on precipitation was extended by including the lower tropospheric 700 and 850hPa compositing levels (not shown). In particular the weighted Pr(ω_{850}) distribution displays a primary maximum for negative ω-bins and a secondary maximum around 20 hPa/day. While the primary maximum confirms that most of the detected precipitation occurs under shallow convection conditions (consistent with observations), a non-negligible contribution is associated with the secondary maximum, indicating in-

tense convection under subsidence dynamical conditions in the low troposphere, which is clearly a model bias. A detailed explanation of the behavior exhibited by this single model is beyond the scope of the present work. However, it is worth to mention that the GISS-ER is an outlier within the IPCC AR4 ensemble, as documented elsewhere. In particular, Lin (2007) reveals that this model features a *permanent El Niño*-like mean SST pattern, with almost no east-west SST gradient in the tropical Pacific, and exceedingly high precipitations over the eastern Pacific.

5 AMIP simulations

The regime analysis performed on the coupled models highlighted the role of convective events of moderate intensity on the set-up of the DI. Specifically, the coupled systems appear to reside in a region of the parameter space characterised by convective regimes for a longer time compared to what is known from observations. In order to single out the effects of the ocean-atmosphere coupling on the DI bias from the contribution deriving from the atmospheric component of the coupled model, we analyse the DI structure in the available AMIP simulations of the Twentieth Century stored at the PCMDI. Compared to the full set of coupled model experiments, the AMIP experiments constitute a smaller 13-members ensemble. Each AMIP simulation has been performed using observed SSTs as a lower boundary condition for the atmospheric model in a stand-alone configuration. The mean seasonal cycle of precipitation in the eastern tropical Pacific for the AMIP ensemble is shown in Fig. 10. As expected, the SST-forced experiments show a reduced inter-model spread, compared to the CGCM ensemble. All of the examined simulations display a reasonable agreement with the observations (except for the IAP model, revealing an overall weak precipitation signal, a feature shared by the corresponding coupled simulation), with no pronounced seasonal excursion of the ITCZ in the Southern Hemisphere. The regime analysis previously applied to the coupled ensemble is now extended to the AMIP simulations. The PDF of the ω_{500} for models and observations is shown in Fig. 11 (left panel). In order to facilitate a direct comparison with the coupled systems

the PDFs of the corresponding CGCM simulations are also shown (Fig. 11, right panel). AMIP runs considerably overestimate the frequency of occurrence of subsidence regimes around the 20 hPa/day peak with respect to both observations and coupled models leading to a generally higher *kurtosis* of the ω_{500} distributions. The most striking difference between AMIP and coupled simulations lies in the larger frequency of occurrence of deep convection regimes featured by the CGCM experiments, basically reflecting the previously emphasized discrepancies between coupled models and observations. Regime sorted precipitations in AMIP and in the corresponding coupled runs are overall consistent in both distribution and magnitude (Fig. 12). The reduced occurrence of deep convection events displayed by AMIP experiments when compared to coupled simulations leads to a consistently reduced inter-model spread of ω_{500}-weighted regime sorted precipitations (Fig. 13). The clusters previously identified for the coupled ensemble collapse into one single behavioural group (essentially reproducing the SUB cluster features) when the AMIP set of experiments is considered.

6 SST–large-scale circulation relationship.

The intercomparison between coupled and AMIP simulations revealed that the SST constraint plays a crucial role in controlling the frequency of occurrence of convective regimes and, as a consequence, on the strength of the spurious precipitation signal in the eastern Pacific. In order to establish in a more quantitative way the relation between the onset of deep convection and the thermal conditions of the surface ocean, the regime sorting approach is here extended to the ω_{500}-SST physical space, so as to obtain ω_{500} distributions sorted by surface thermal regimes. This analysis allows to clearly identify SST-thresholds leading to the onset of deep convection events for each model.

Using the same procedure outlined in section 4, the SST domain is split into bins of 0.5 degrees width. Then, the average ω_{500} is computed for each SST bin, over the previously defined longitude-latitude box. The model ω_{500} distributions sorted by thermal regimes

display a typical elbow-like pattern which is qualitatively consistent with the observed one (Fig. 14; see also Bony et al., 1997; Lau et al., 1997). The mid-troposphere vertical velocity is typically positive (indicating subsidence conditions) and approximately constant for surface temperatures lower than a threshold value, beyond which the system enters into a different dynamical regime characterised by deep convection. A (model dependent) critical SST leading to the regime transition is here simply identified as the surface temperature corresponding to the zero-crossing of the regime sorted ω_{500}. Alternative options are clearly possible, the most obvious one being the SST corresponding to the elbow in the thermally-sorted ω_{500} curve. However, the latter can be potentially affected by large uncertainties, due to the smooth transition displayed by some of the model realizations. Moreover, the zero-crossing criterion applied to the adopted dynamical proxy objectively separates subsidence from ascending conditions.

The vast majority of AR4 models display a regime transition for temperatures which are lower than the observed 28^{o}C threshold, with a relatively large spread within the 26-29.5 ^{o}C range. The intra-model scatter displayed by the zero-crossing SSTs clearly reflects the differing sensitivities of deep convection on ocean surface thermal conditions displayed by the various coupled models. In order to establish whether the thermal conditions of the surface ocean are more likely to lie beyond or below the corresponding model SST threshold, we need to associate to each thermal regime the corresponding frequency of occurrence. The PDF for each selected SST bin (shown in Fig. 15) reveals a wide spectrum of model SST distributions, symmetrically spread around the observed distribution. Combining together the SST corresponding to the most likely thermal state (i.e., the SST corresponding to the PDFs peak in Fig. 15; hereafter MLT) with the SST threshold previously identified (hereafter THR), it is possible to estimate the likelihood for a given model to undergo a deep convection event, in the examined region. In other words, models whose most likely thermal state is warmer (colder) than THR are more (less) likely to be in the deep convection region of the phase space. In Fig. 16, the difference between THR and MLT is shown for models and observations. Negative (positive) values in Fig.

16 correspond to models whose SST is most of the time warmer (colder) than the deep convection threshold, and are thus expected to feature a more (less) pronounced bias on precipitation. Almost all of the models pertaining to the previously identified INT and HYBRID clusters lie below the zero line. Three of them (IAP, IPSL and NCAR CCSM3) display a positive value for this index, although they are very close to the zero limit. On the other hand, all of the models showing a THR-MLT difference $\geq 1^o$ fall within the SUB model group.

In order to further corroborate the hypothesis of a strict relationship between the DI systematic error and the THR-MLT index, models are displayed in the 2-dimensional parametric space definded by the SI index, defined in section 3, and the THR-MLT index (Fig. 17). Here, the split between the SUB (low DI bias, positive THR-MLT) and HYBRID and INT (strong DI bias, negative or marginally positive THR-MLT) model populations appears to be more evident. The grossly linear relationship emerging between these two indices (correlated at the 0.84 level) suggests causality between the amplitude of the systematic error on precipitation and the combined bias on the critical SST leading to deep convection and on the surface thermal state in the south-eastern Pacific. Consistent with this interpretation, models displaying a DI persisting through most of the year (Fig. 1) are those whose surface temperatures are prone to be systematically warmer than the SST threshold leading to the onset of deep convection. On the other hand, a large THR-MLT difference acts as a deterrent for the start of deep convection. The UKMO HADCM3 model provides a particularly insightful example, as it features an overly large THR (29.5 ^{o}C) combined with a MLT consistent with the observed one, leading to a fairly reduced DI error. Different reasons (i.e., a THR close to observations, and a cold-biased MLT) induce a similar performance in the UKMO HADGEM1 model.

7 Summary and conclusions

In this study the double-ITCZ systematic error affecting the climate of the tropical eastern Pacific in the current generation of coupled models is examined in relation with the rep-

resentation of atmospheric vertical circulation regimes, using a regime sorting approach. The analysis, applied to both coupled and uncoupled (atmosphere-only) IPCC AR4 simulations of the twentieth century, reveals that the excess of precipitation detected in the south-eastern Pacific (the DI region) in CGCMs is mainly due to the overly frequent onset of deep convection, whereas the error on rainfall magnitude associated with individual convective events is overall consistent with errors already present in the corresponding AMIP-type simulations. Through the present analysis we also identified three distinct model behavioural groups within the AR4 ensemble, thus associating to each model a DI rainfall fingerprint: two unimodal distributions, SUB and INT, featuring maximum precipitation under subsidence and deep convection regimes respectively, and one bimodal distribution, HYBRID, displaying both components. A simple metric for precipitation, based on the model-observation root-mean-square error, but defined in the vertical circulation regime space, reveals that models which correctly capture (at least, qualitatively) the observed regime-sorted rainfall pattern in the eastern Pacific (SUB cluster) do also minimize the RMSE. Thus, the most intense DI occurrences are associated with the spurious deep convective precipitation *bulge* in the ω_{500}-space displayed by models in the INT and HYBRID clusters. The relative homogeneity displayed by CGCMs in the DI precipitation signature sharply contrasts with the richness of deep convection schemes (and corresponding closure/triggers) adopted by individual climate models in the AR4 ensemble (see Table 1 in Lin 2007 for a synoptic view). Each single identified cluster displays a wide variety of deep convection parameterizations (not shown), thus there is no obvious relationship between a given model group and a specific deep convection scheme. Clearly, the AR4 experimental set is not optimal in that different realizations of the twentieth century climate are produced with model configurations differing by several aspects (parameterisations of unresolved processes, spatial resolution, dynamical cores, etc.) so that intra-model differences can be hardly ascribed to one single element, but may rather result from the additional effect of changing many different model features (Schneider 2002). However, the apperent lack of sensitivity to convective schemes shown

by models within each single cluster seems to indicate that there is a more fundamental factor overcoming the differences between the adopted deep convection schemes, and thus forcing very different systems to behave in a similar way. As pointed out in previous studies, SST is a primary candidate to explain the DI location and strength in both observations (Zhang, 2001) and models (Mechoso et al. 1995; Yu and Mechoso, 1999). Relative maxima in SST control the regions where the largest upward vertical motions occur (Schneider, 1977), which are in turn responsible for the vertical advection of moisture, an important pre-requisite for the onset of deep convection. The comparison between coupled and AMIP experiments further confirms that it is the drift of surface thermal conditions from a realistic pattern to determine the intra-model spread in the manifestation of DIs, as GCMs behavioural clusters collapse into one single group under prescribed SSTs. This suggests that the existence of homogeneous CGCMs classes can be traced back to the different ways the coupled models represent the SST-deep convection relationship.

The composite analysis of ω_{500} in the space defined by surface thermal states shows that the critical SST setting the transition to deep convective unstable conditions in the AR4 models population can vary within a wide range of values, likely reflecting the aforementioned variety of deep convection schemes featured by climate models. Similarly, the SST biases in tropical Pacific do also exhibit a large intra-model scatter. However, a model displaying anomalously warm surface temperatures over the eastern Pacific does not necessarily favour the onset of deep convection (thus producing overly strong precipitations) unless the corresponding convective SST threshold lies, on average, below the surface temperature in that region. Thus, the distance between the critical convective SST and the average SSTs over the DI region largely control the model clustering process. This result is consistent with the finding that model SSTs in the tropical eastern Pacific are symmetrically distributed around the observations (within a belt about 2^oC wide), while precipitation is systematically higher than the observational estimates (Fig. 6 and 15; see also Fig. 2 in de Szoeke and Xie, 2008). The symmetric model SST distribution indicates that cold-biased models can in principle result in anomalously large rainfall and spuri-

ous southern ITCZ, if the convective SST-threshold is consistently lower than the average SST. Specularly, a warm-biased model may display unfavourable conditions to the set-up of anomalous deep convection if the SST threshold for deep convection is sufficiently larger than the mean SSTs in the eastern Pacific (see the HadCM3 case).

Summarizing, an important outcome of this study is that, by splitting the total DI bias on precipitation into 1) an error on the frequency of occurrence of deep convection, and 2) an error on the magnitude of precipitation for an individual convective event, it is possible to state that the first is caused by ocean-atmosphere interactions, whereas the second can be attributed to the atmospheric GCM component only, with the former playing a major role on the total amplitude of the DI bias.

A dominant paradigm among the theories trying to explain the DI in climate models invokes the well know deficit of low level stratocumulus clouds in the south-eastern Pacific (Philander et al., 1996; Yu and Mechoso, 1999). The lack of stratocumuls clouds and the implied enhancement of solar radiation income do in turn determine a warm bias at the ocean surface which ultimately triggers deep convection and precipitation, in a region where the observed dominant regime is subsidence with consistently low rainfall. However, a closer look at the zonally averaged mean meridional SST profile in the region under exam reveals that not all of the models display a warm bias therein, but there is a rather symmetric scatter of warm and cold SST biases around the observations (see Fig. 2 in deSzoeke and Xie, 2008). Precipitation, on the other hand, are mostly skewed towards positive anomalies with almost all of the models overestimating precipitation in the tropical south-eastern Pacific. Assuming a thermally-driven nature for the DI bias, with the present analysis we suggest a possible explanation for the above mentioned apparent inconsistency between SST and precipitation biases, with the missing link identified in the model-dependent critical SST setting the transition to a deep convective regime. This parameter partly decouples the SST bias from the bias on precipitation, as models with a cold bias may still be featuring overly strong rainfall, provided that their convective SST-threshold is consistently low.

While the local impact of SSTs is in our view a major driver of the DI sytematic error, the analysis of the AMIP simulations (section 5) suggests that the constraint of SSTs over regions which are far from the eastern Pacific may exert a similarly important control on the rainfall bias over the examined region. The non-local factor which most likely influences the tropical rainfall pattern in an atmospheric stand-alone simulation with prescribed observed SSTs is related to the presence of a correct SST-gradient across the equator. Numerical experiments performed using AGCMs with simplified water-covered Earth configurations forced by idealized zonally symmetric SST profiles (Aqua-Planet Experiment Project; http://www.pcmdi.llnl.gov/projects/amip/ape) suggest that transitions from a single to a double-ITCZ equilibrium may arise (at least in some models) after gradually reducing the SST meridional gradient (from *peaked* to *flat*) around the equator. However, the large inter-model spread in AGCMs' response to idealized SST-gradients cast large uncertainties as to the precise mechanisms governing the relation between the non-local SST forcing and the latitudinal ITCZ location.

DIs have been found to be largely controlled by the combined effect of SST-deep convection coupling, and the amplitude of the SST bias in the eastern Pacific. The SST threshold setting the transition to deep convection, even if not directly disposable may be partly controlled through an appropriate modeling of the triggers characterizing a given deep convection scheme. The criteria used to determine the initiation of convection considerably vary from one scheme to another, including cloud-base buoyancy (Gregory and Rowntree, 1990), moisture convergence (Tiedtke, 1989) and convective available potential energy (Zhang and McFarlane, 1995), to mention a few. Each of these quantities is ultimately controlled by SST via processes occurring in the boundary layer. Revisiting the deep convection schemes used by AR4 models in view of the above considerations may represent a possible pathway to alleviate the DI syndrome in CGCMs. This will require additional efforts, including numerical experiments to be performed by individual modeling groups, specifically designed to address errors in the representation of SST-deep convection coupling and their impact on the double-ITCZ bias.

The construction of a set of standard metrics aimed to evaluate climate models performance is a most urgent need, as the multi-model intercomparison framework is becoming a standard procedure in climate science. A wide consensus is emerging on the fact that application-dependent metrics are more valuable and physically justifiable compared to single indices of the overall model performance, as the latter are tipically based on a somewhat arbitrary set of non-homogeneous metrics (Gleckler et al., 2007). The onset of a split ITCZ is a bias affecting the vast majority of state-of-the-art CGCMs in a region which is crucial to the development of El Niño. Thus, building a specific metric to rank models with respect to this particular systematic error is a relevant step towards the definition of a set of process-oriented metrics. The regime sorting methodology has been found to be a particularly insightful instrument in the diagnosis of double-ITCZs in CGCMs. Metrics based on this approach may represent a useful complement to existing diagnostics in the assessment of models ability to reproduce the climate of the tropics, within the framework of upcoming multi-model intercomparison efforts.

Acknowledgements. Stimulating discussions with Erich Roeckner, Pascale Braconnot and the participants of the WGNE Workshop on Systematic Errors in Climate and NWP Models held in San Francisco on February 2007 are acknowledged. This paper was partially supported by the Italy-US cooperation on climate change science and technolgy, funded by the italian Ministry of Environment and Protection of Land and Sea, and by the EU ENSEMBLES Project (Contract GOCECT-2003-505539).

References

Bony S.,K.M. Lau, and Y.C. Sud, 1997: Sea surface temperature and large-scale circulation influences on tropical greenhouse effect and cloud radiative forcing. *J. Climate,* **10,** 2055–2077.

Bony S.,J.L. Dufresne, H. Le Treut, J.J. Morcrette, and C. Senior, 2004: On dynamic and thermodynamic components of cloud changes. *Clim. Dyn.,* **22,** 71-86.

Charney, J.G., 1971: Tropical cyclogenesis and the formation of the Intertropical Convergence Zone. *Mathematical Problems of Geophysical Fluid Dynamics,* W.H. Reid, Ed., *Lectures in Applied Mathematics,* Vol. 13, Amer. Math. Soc., 355–368.

Chéruy F., and F. Chevallier, 2000: Regional and seasonal variations of the clear-sky atmospheric longwave cooling over tropical oceans. *J. Climate,* **13,** 2863–2875.

de Szoeke S.P. and P. Xie, 2008: The tropical eastern pacific seasonal cycle: assessment of errors and mechanisms in IPCC AR4 coupled ocean-atmosphere general circulation models. *J. Climate,* **21,** 2573–2590.

Gleckler P., M. Miller, J. Hack, D. Bader, K. Sperber and K. Taylor, 2007: Summary of the 3rd WGNE Workshop on Systematic Errors in Climate and NWP Models. UCRL-TR-403078, Lawrence Livermore National Laboratory, Livermore, CA, 8pp.

Gregory D., and P.R. Rowntree, 1990: A mass flux convection scheme with representation of cloud ensembles characteristics and stability-dependent closure. *Mon. Wea. Rev.,* **118,** 1483–1506.

Hayashi, Y.-Y., and A. Sumi, 1986: The 30-40 day oscillation simulated simulated in an “Aqua Planet” model. *J. Meteor. Soc. Japan,* **64,** 451–465.

Hess P.G, D.S. Battisti and P. Rasch, 1993: Maintenance of the Intertropical Convergence Zones and the large-scale tropical circulation on a water-covered Earth. *J. Atmos. Sci.,* **50,** 691–713.

Holton J.R., J.M. Wallace and J.A. Young, 1971: On boundary layer dynamics and the ITCZ. *J. Atmos. Sci.,* **28,** 275–280.

Hourdin F., and Coworkers, 2006: The LMDZ4 general circulation model: climate performance and sensitivity to parametrized physics with emphasis on tropical convection. *Clim. Dyn.,* **27,** 787–813.

Lau, N.-C., I.M. Held and J.D. Neelin, 1988: The Madden-Julian oscillation in an idealized general circulation model. *J. Atmos. Sci.,* **45,** 3810–3832.

Lau, N.-C., H.-T. Wu and S. Bony, 1997: The role of large-scale atmospheric circulation in the relationship between tropical convection and sea surface temperature. *J. Climate,* **10,** 381–392.

Lin J.L., 2007: The double-ITCZ problem in IPCC AR4 coupled GCMs: ocean-atmosphere feedback analysis. *J. Climate,* **20,** 4497-4525.

Mechoso C.R., A.W. Robertson, N. Barth, M.K. Davey, P. Delecluse, P.R. Gent, S. Ineson, B. Kirtman, M. Latif, H. Le Treut, T. Nagai, J.D. Neelin, S.G.H. Philander, J. Polcher, P.S. Schopf, T. Stockdale, M.J. Suarez, L. Terray, O. Thual, and J.J. Tribbia, 1995: The seasonal cycle over tropical pacific in coupled ocean-atmosphere general circulation models, *Mon. Wea. Rev.,* **123,** 2825–2838.

Meehl, G.A., C. Covey, B. McAvaney, M. Latif, and R.J. Stouffer, 2005: Overview of the Coupled Model Intercomparison Project. *Bull. Amer. Meteor. Soc.,* **86,** 89–93.

Philander S. G. H., D. Gu, D. Halpern, G. Lambert, N.-C. Lau, T. Li, and R.C. Pacanowski, 1996: Why the ITCZ is mostly north of the equator. *J. Climate,* **9,** 2958–2972.

Rayner, N. A., D. E. Parker, E. B. Horton, C. K. Folland, L. V. Alexander, D. P. Rowell, E. C. Kent, and A. Kaplan, 2003: Global analyses of sea surface temperature, sea ice, and night marine air temperature since the late nineteenth century. *J. Geophys. Res.,* **108**(D14), 4407, doi:10.1029/2002JD002670.

Schneider, E.K., 1977: Axially symmetric steady-state models of the basic state for instability and climate studies. Part II. Nonlinear calculations. *J. Atmos. Sci.,* **34,** 280-296.

Schneider, E.K., 2002: Understanding differences between the equatorial Pacific as simulated by two coupled GCMs. *J. Climate,* **15,** 449-469.

Swinbank, R., T.N. Palmer and M.K. Davey, 1988: Numerical simulations of the Madden and Julian oscillation. *J. Atmos. Sci.,* **45,** 774–788.

Tiedtke, M., 1989: A comprehensive mass flux scheme for cumulus parameterization in large-scale models. *Mon. Wea. Rev.,* **117,** 1779–1800.

Uppala S., and Coworkers, 2005: The ERA-40 reanalysis. *Q.J.R. Meteorol. Soc.,* **131,** 2961–3012.

Waliser D., and R.C.J. Somerville, 1994: Preferred latitudes of the intertropical convergence zone. *J. Atmos. Sci.*, **51,**12, 1619–1639.

Xie P., and P.A. Arkin, 1997: Global precipitation: A 17-year monthly analysis based on gauge observations, satellite estimates, and numerical model outpus. *Bull. Am. Meteor. Soc.*, **78,**11, 2539–2558.

Yu J.-Y., and C. Mechoso, 1999: Links between annual variations of Peruvian stratocumulus clouds and of SST in the eastern equatorial Pacific. *J. Climate,* **12,** 3305–3318.

Zhang G.J., and N.A. McFarlane, 1995: Sensitivity of climate simulations to the parameterization of cumulus convection in the CCC-GCM. *Atmos.-Ocean*, **3,** 407–446.

Zhang C., 2001: Double ITCZs. *J. Geophys. Res.*, **106**(D11), 11785-11792.

Tables

Modeling Group	Model Label	Flux Adjustment
Bjerknes Centre for Climate Research (Norway)	BCCR	No
Canadian Centre for Climate Modelling and Analysis	CCCMA T47	Heat,Water
Canadian Centre for Climate Modelling and Analysis	CCCMA T63	Heat,Water
Centre National de Recherches Meteorologiques (France)	CNRM	No
CSIRO Atmospheric Research (Australia)	CSIRO	No
NOAA/Geophysical Fluid Dynamics Laboratory (United States)	GFDL CM2-0	No
NOAA/Geophysical Fluid Dynamics Laboratory	GFDL CM2-1	No
NASA Goddard Institute for Space Studies (United States)	GISS AOM	No
NASA Goddard Institute for Space Studies	GISS EH	No
NASA Goddard Institute for Space Studies	GISS ER	No
LASG/Institute of Atmospheric Physics (China)	IAP	No
Istituto Nazionale di Geofisica e Vulcanologia (Italy)	INGV	No
Institute for Numerical Mathematics (Russia)	INMCM3	Water
Institute Pierre Simon Laplace (France)	IPSL CM4	No
Centre for Climate System Research (Japan)	MIROC HIRES	No
Centre for Climate System Research	MIROC MEDRES	No
Meteorological Institute of the University of Bonn (Germany)	MIUB	Heat,Water
Max Planck Institute for Meteorology (Germany)	MPI	No
Meteorological Research Institute (Japan)	MRI	Heat, Water
Hadley Centre for Climate Prediction and Research, Met Office (United Kingdom)	UKMO HADGEM1	No
Hadley Centre for Climate Prediction and Research, Met Office	UKMO HADCM3	No
National Centre for Atmospheric Research (United States)	NCAR PCM1	No
National Centre for Atmospheric Research	NCAR CCSM3	No

Table 1: List of the models analysed in this study.

Figure Captions

Fig. 1. Mean seasonal cycle of precipitation over the eastern Pacific (averaged between 150W and 100W) plotted against latitude. Contour interval is 2 mm/day, with values greater than 6 mm/day stippled.

Fig. 2. SI index (mm/day; see text for details) for each member of the extended (23 members) AR4 ensemble and observations sorted in ascending order of index magnitude. Squares (crosses) indicate persistent DI (alternating ITCZ) error, while Xie-Arkin data are indicated with a circle. Flux corrected models are further labelled with stars.

Fig. 3. Mean seasonal cycle of the lagrangian pressure tendency at 500 hPa (ω_{500};in hPa/day) for the IPCC AR4 models, in [150W-100W,20S-0].

Fig. 4. Mean precipitation (in mm/day) versus mean lagrangian pressure tendency at 500 hPa (ω_{500};in hPa/day) for the IPCC AR4 models in [150W-100W,20S-0], time-averaged over JFMAMJ (white circles) and JASOND (black circles). Stars indicate corresponding ERA40/Xie-Arkin values.

Fig. 5. Probability density function of ω_{500} in the [150W-100W,20S-0] longitude-latitude range for AR4 models and observations (ERA40). Model PDFs are computed from monthly outputs from the 1960-2000 period of IPCC 20C3M simulations.

Fig. 6. Composite of precipitation (mm/day) for different vertical circulation regimes identified by ω_{500}, in the [150W-100W,20S-0] longitude-latitude range for AR4 models and Xie-Arkin data set.

Fig. 7. Regime sorted precipitation (mm/day) weighted by the PDF of ω_{500}, for AR4 models and observations.

Fig. 8. Regime sorted precipitation (mm/day) weighted by the PDF of ω_{500}, for model cluster SUB (left), INT (middle) and HYBRID (right). Legend as in figure 5.

Fig. 9. RMSE of regime sorted precipitation (mm/day) for different model clusters (see text for details).

Fig. 10. Mean seasonal cycle of precipitation over the eastern Pacific (averaged between 150W and 100W) plotted against latitude for AMIP simulations and observations. Contour interval is 2 mm/day, with values greater than 6 mm/day stippled.

Fig. 11. Probability density function of ω_{500} in the [150W-100W,20S-0] longitude-latitude range for AMIP (left) and corresponding coupled (right) simulations.

Fig. 12. Composite of precipitation (mm/day) for different vertical circulation regimes identified by ω_{500}, in the [150W-100W,20S-0] longitude-latitude range for AMIP (left) and corresponding coupled (right) simulations.

Fig. 13. Regime sorted precipitation (mm/day) weighted by the PDF of ω_{500}, for AMIP (left) and corresponding coupled (right) simulations.

Fig. 14. Composite of ω_{500} (hPa/day) sorted by surface temperature regimes (^{o}C).

Fig. 15. Probability density function of sea surface temperature in the [150W-100W,20S-0] longitude-latitude range for AR4 models and observations (HadISST). Model PDFs are computed from monthly outputs from the 1960-2000 period of IPCC 20C3M simulations.

Fig. 16. Difference between THR and MLT temperature for models and observations (see text for details). Colors indicate whether the model falls within the SUB (blue), INT (red) or HYBRID (green) cluster. Black is used for observations.

Fig. 17. Scatterplot of THR-MLT (^{o}C) and SI index (mm/day) for models and observations (see text for details). Colors indicate whether the model falls in the SUB (blue), INT (red) or HYBRID (green) cluster. Black is used for observations.

Figures

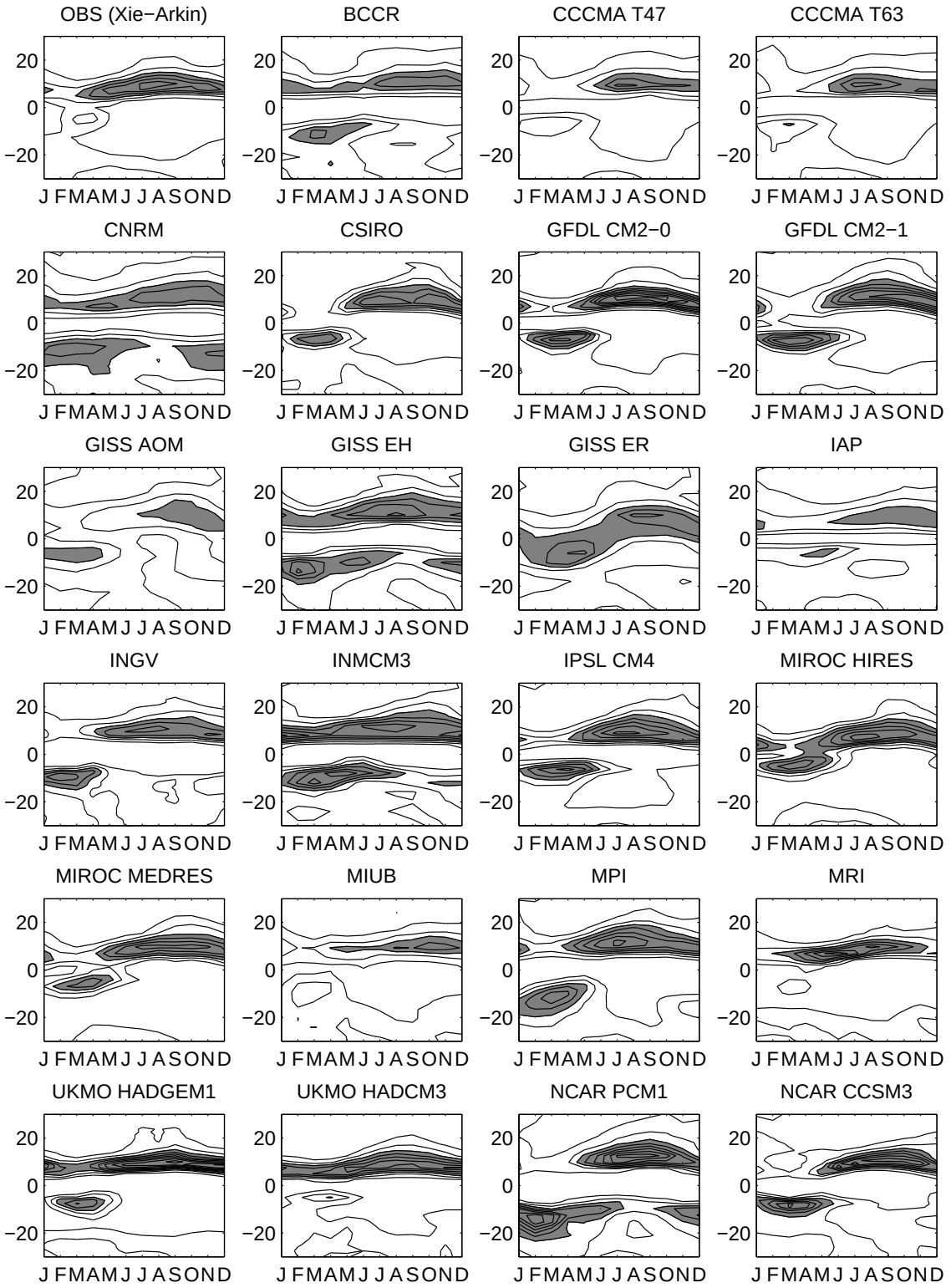

Fig. 1: Mean seasonal cycle of precipitation over the eastern Pacific (averaged between 150W and 100W) plotted against latitude. Contour interval is 2 mm/day, with values greater than 6 mm/day stippled.

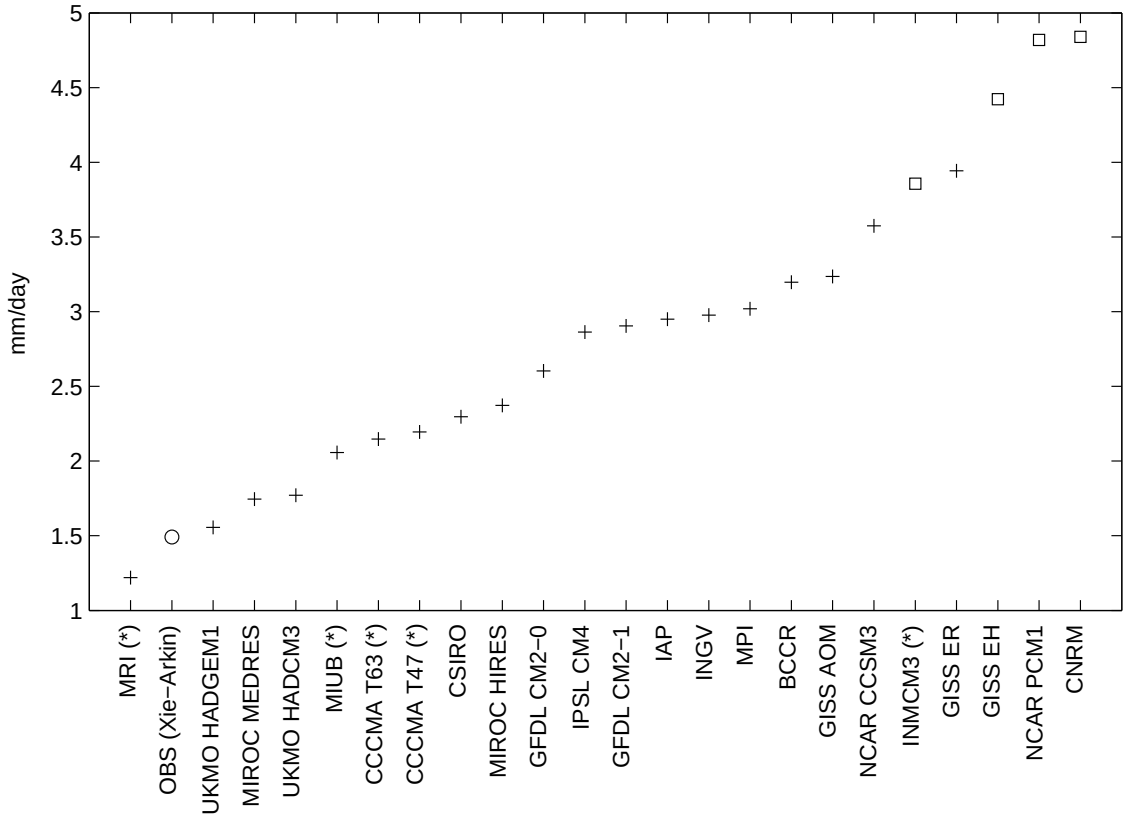

Fig. 2: SI index (mm/day; see text for details) for each member of the extended (23 members) AR4 ensemble and observations sorted in ascending order of index magnitude. Squares (crosses) indicate persistent DI (alternating ITCZ) error, while Xie-Arkin data are indicated with a circle. Flux corrected models are further labelled with stars.

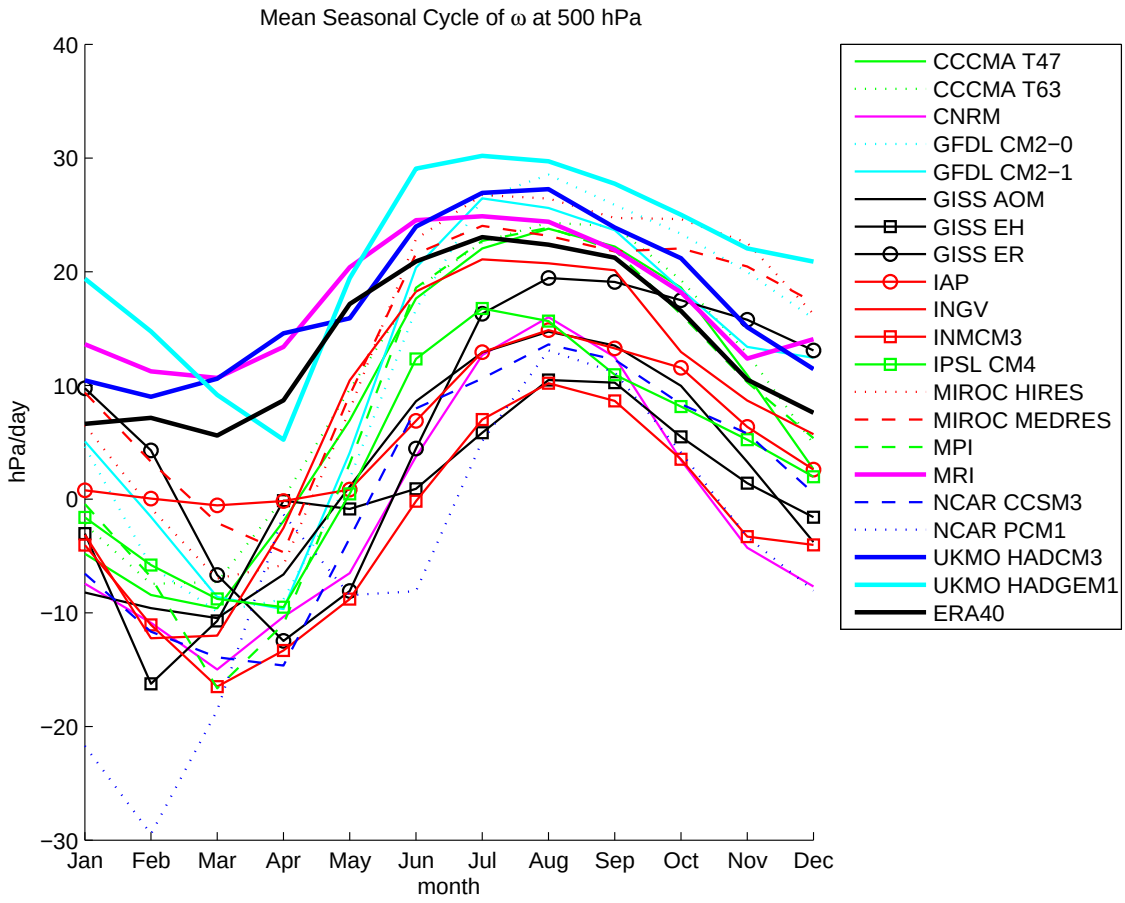

Fig. 3: Mean seasonal cycle of the lagrangian pressure tendency at 500 hPa (ω_{500};in hPa/day) for the IPCC AR4 models, in [150W-100W,20S-0].

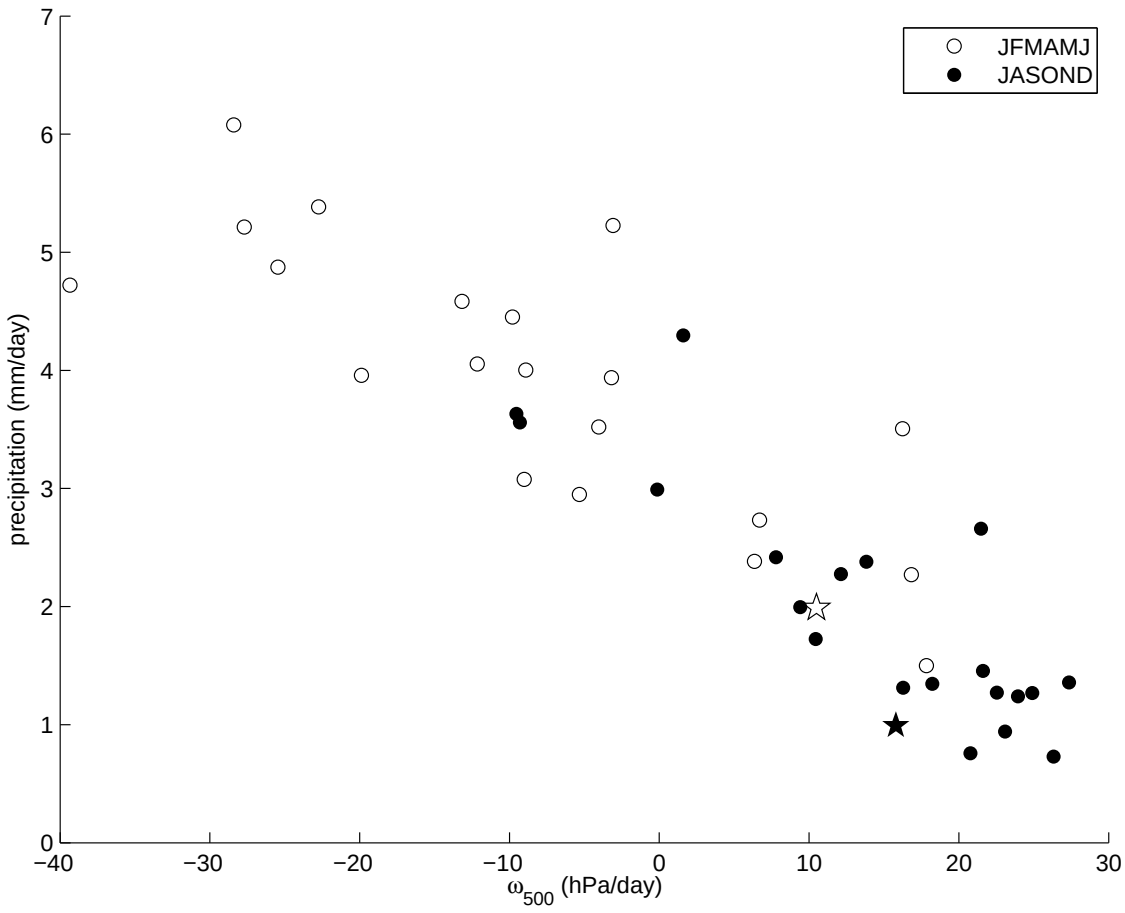

Fig. 4: Mean precipitation (in mm/day) versus mean lagrangian pressure tendency at 500 hPa (ω_{500};in hPa/day) for the IPCC AR4 models in [150W-100W,20S-0], time-averaged over JFMAMJ (white circles) and JASOND (black circles). Stars indicate corresponding ERA40/Xie-Arkin values.

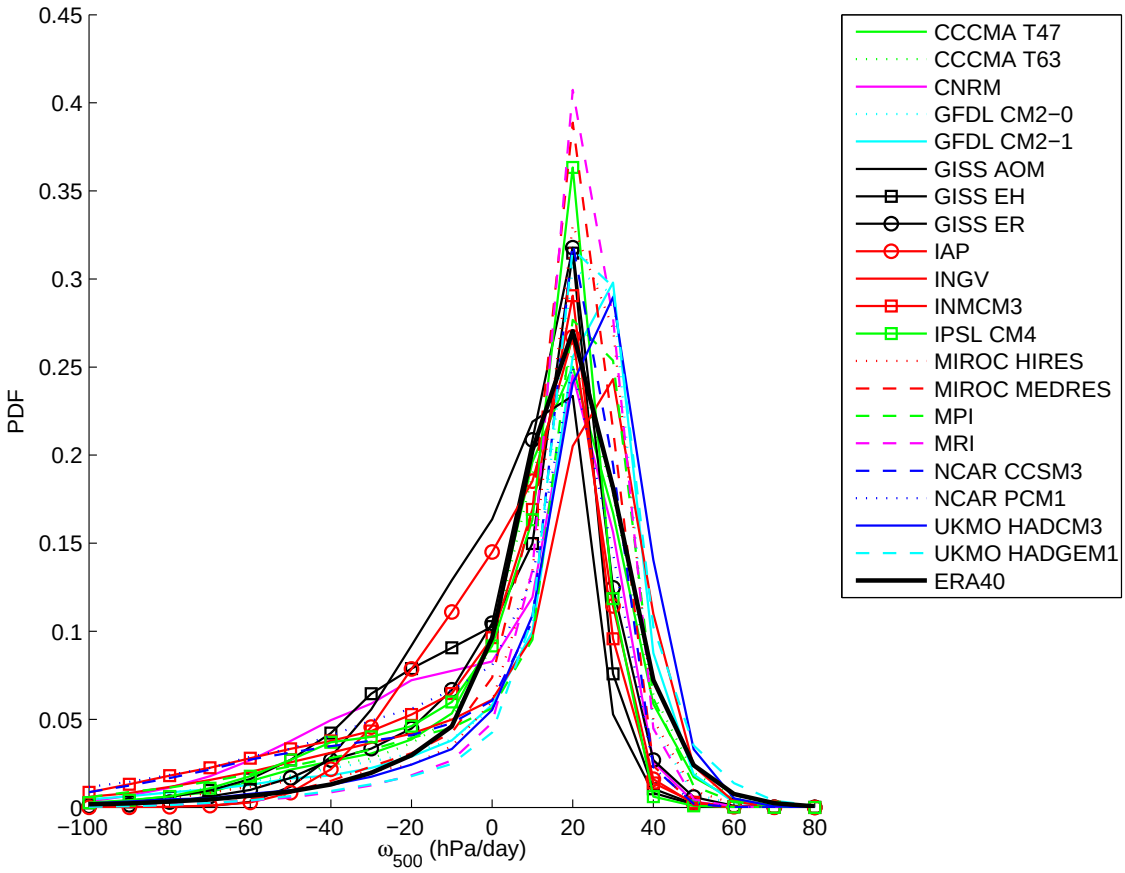

Fig. 5: Probability density function of ω_{500} in the [150W-100W,20S-0] longitude-latitude range for AR4 models and observations (ERA40). Model PDFs are computed from monthly outputs from the 1960-2000 period of IPCC 20C3M simulations.

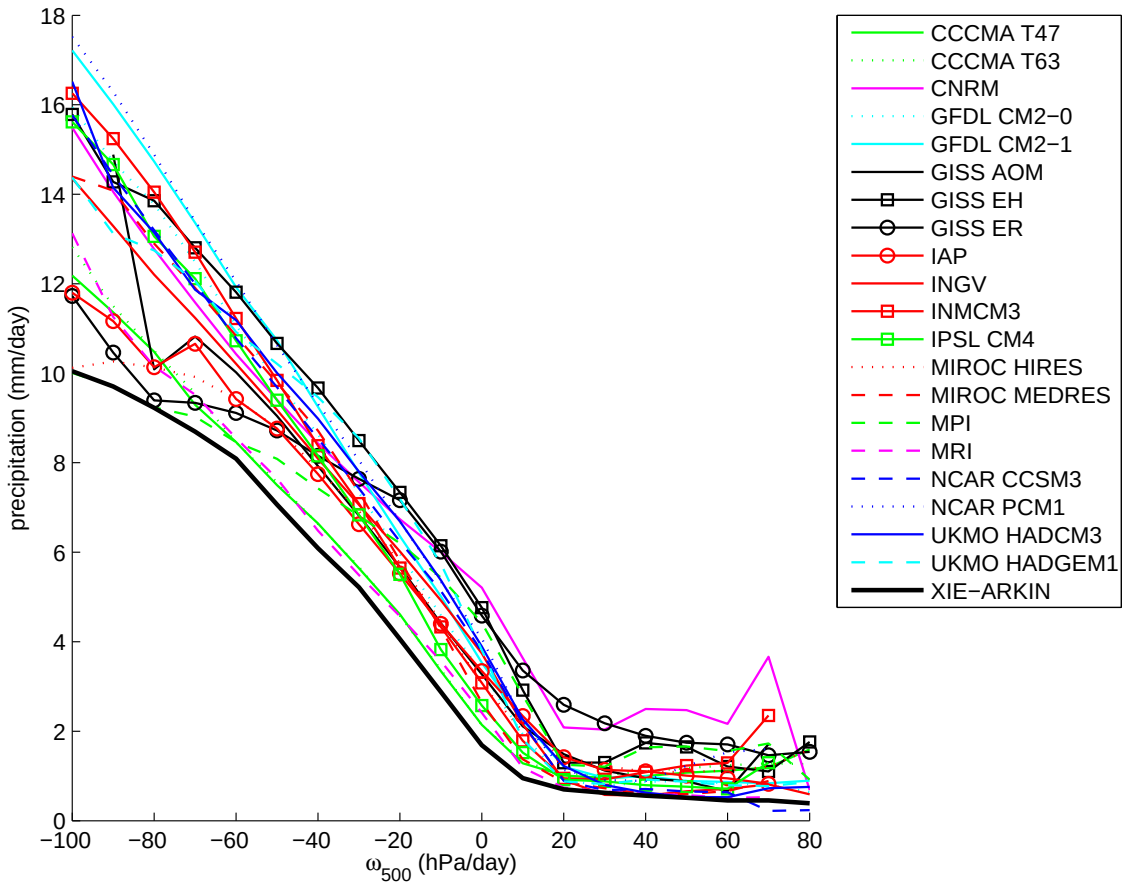

Fig. 6: Composite of precipitation (mm/day) for different vertical circulation regimes identified by ω_{500}, in the [150W-100W,20S-0] longitude-latitude range for AR4 models and Xie-Arkin data set.

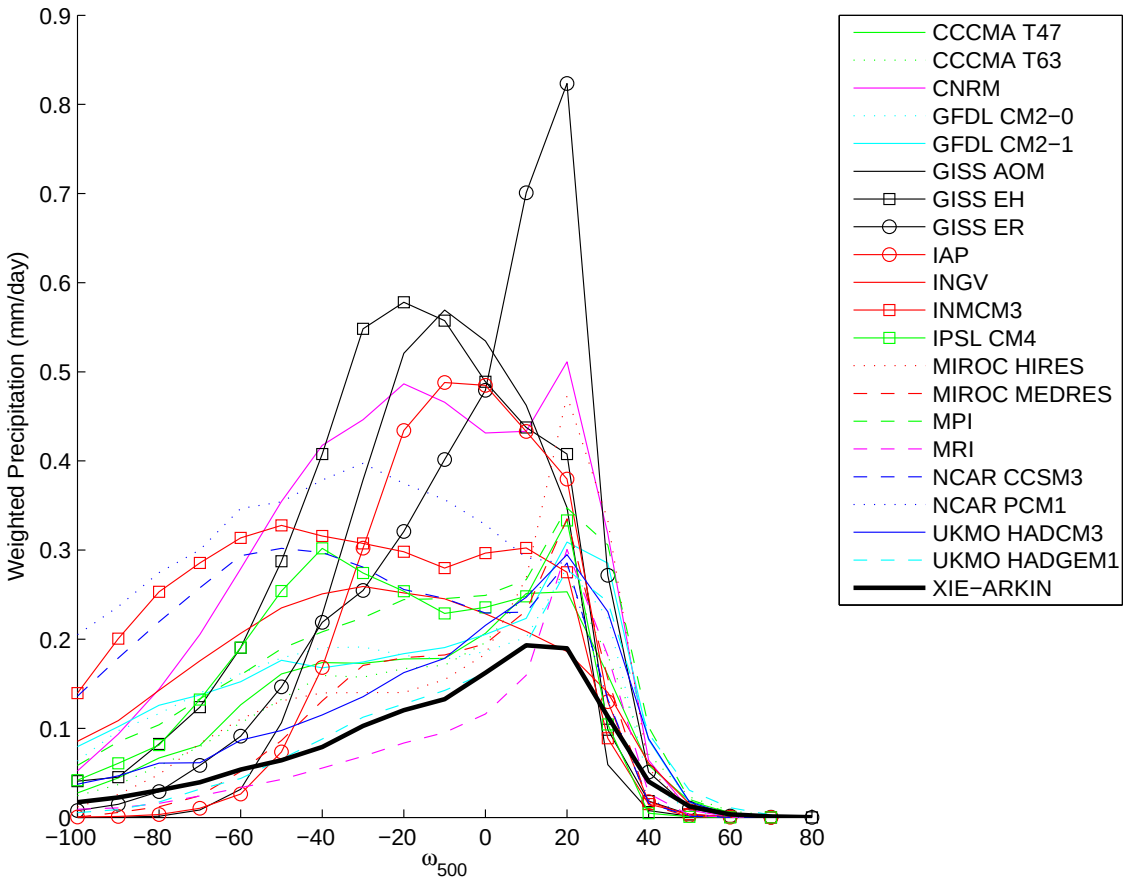

Fig. 7: Regime sorted precipitation (mm/day) weighted by the PDF of ω_{500}, for AR4 models and observations.

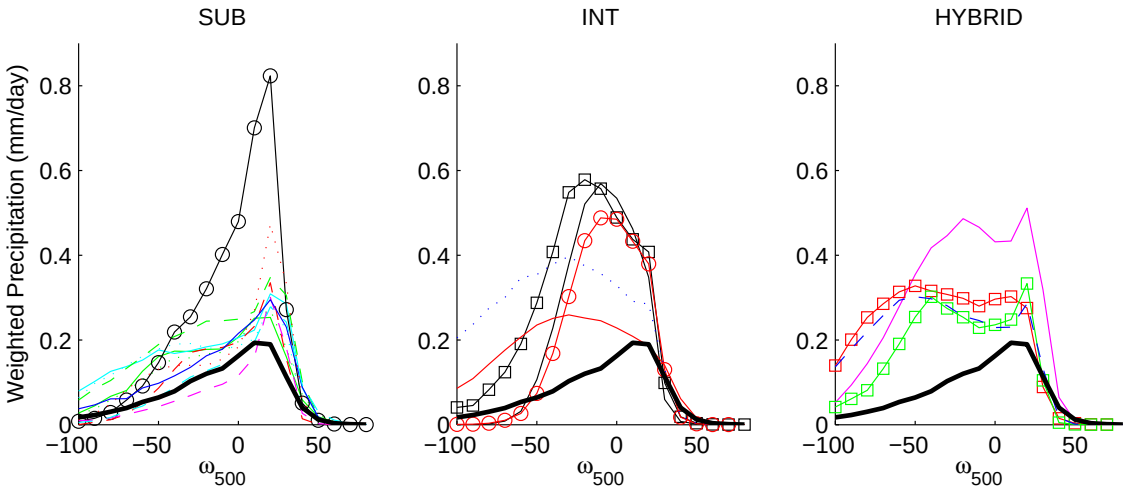

Fig. 8: Regime sorted precipitation (mm/day) weighted by the PDF of ω_{500}, for model cluster SUB (left), INT (middle) and HYBRID (right). Legend as in figure 5.

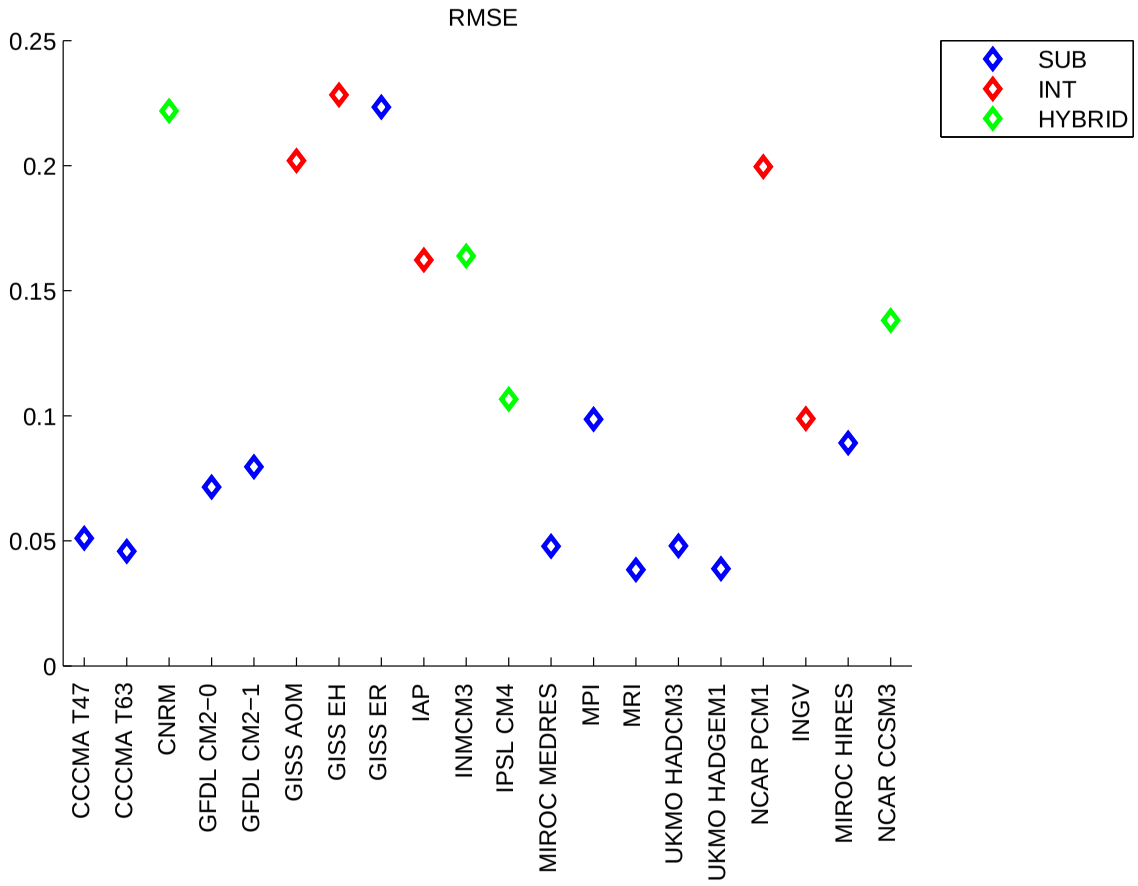

Fig. 9: RMSE of regime sorted precipitation (mm/day) for different model clusters (see text for details).

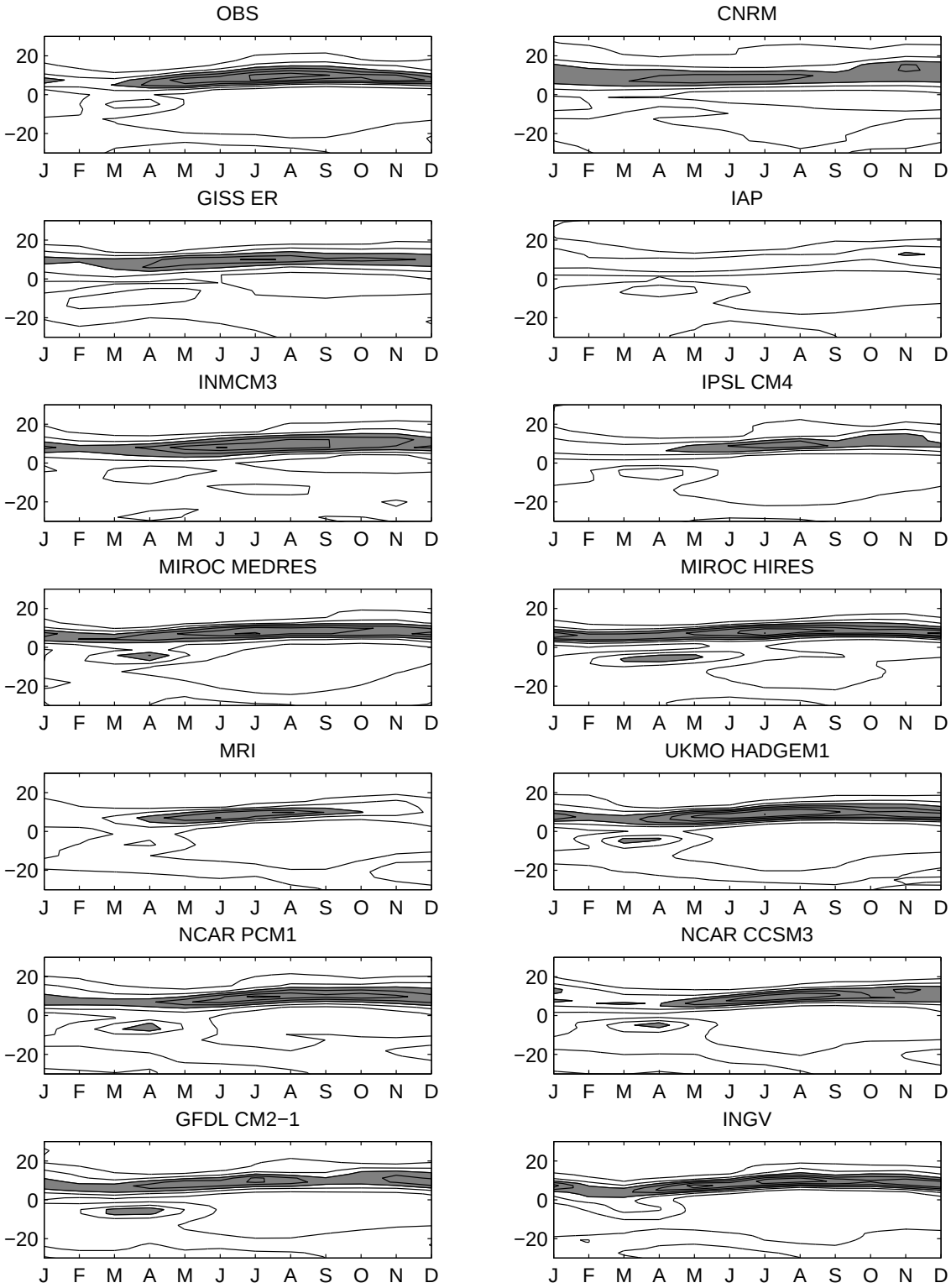

Fig. 10: Mean seasonal cycle of precipitation over the eastern Pacific (averaged between 150W and 100W) plotted against latitude for AMIP simulations and observations. Contour interval is 2 mm/day, with values greater than 6 mm/day stippled.

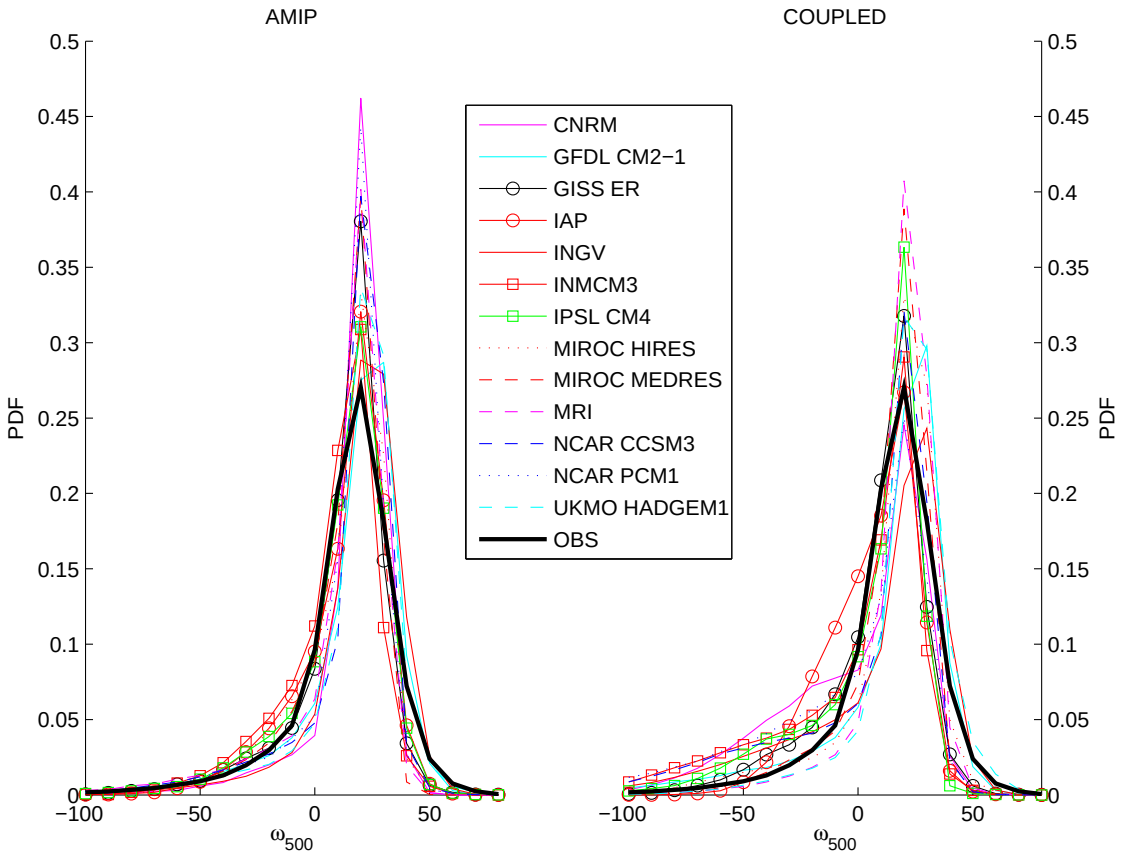

Fig. 11: Probability density function of ω_{500} in the [150W-100W,20S-0] longitude-latitude range for AMIP (left) and corresponding coupled (right) simulations.

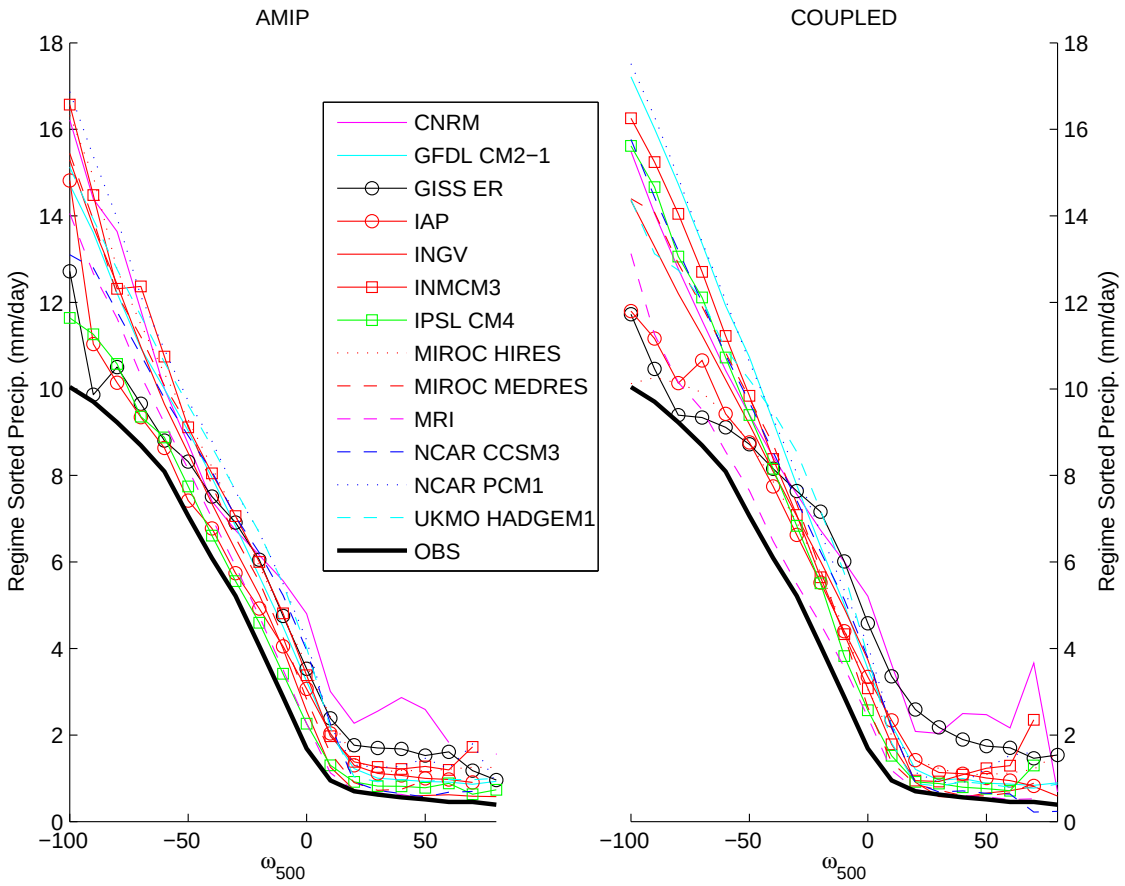

Fig. 12: Composite of precipitation (mm/day) for different vertical circulation regimes identified by ω_{500}, in the [150W-100W,20S-0] longitude-latitude range for AMIP (left) and corresponding coupled (right) simulations.

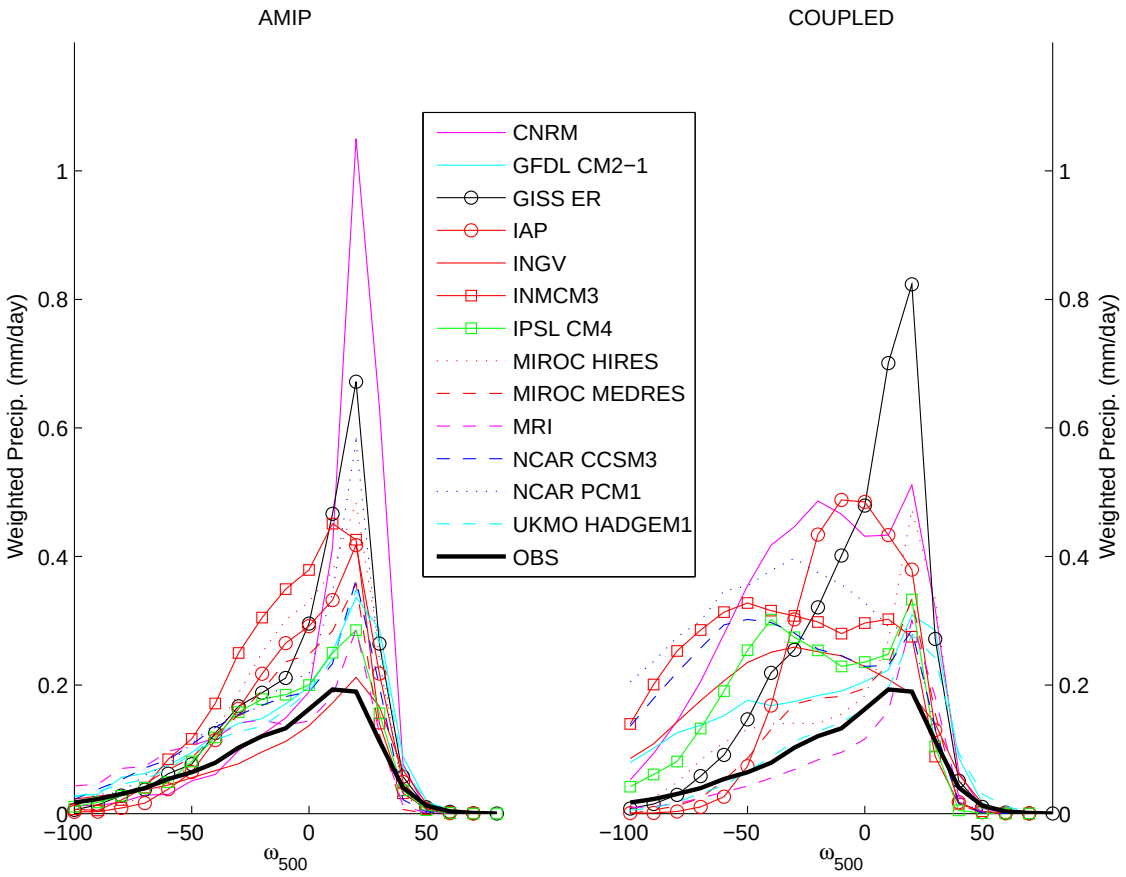

Fig. 13: Regime sorted precipitation (mm/day) weighted by the PDF of ω_{500}, for AMIP (left) and corresponding coupled (right) simulations.

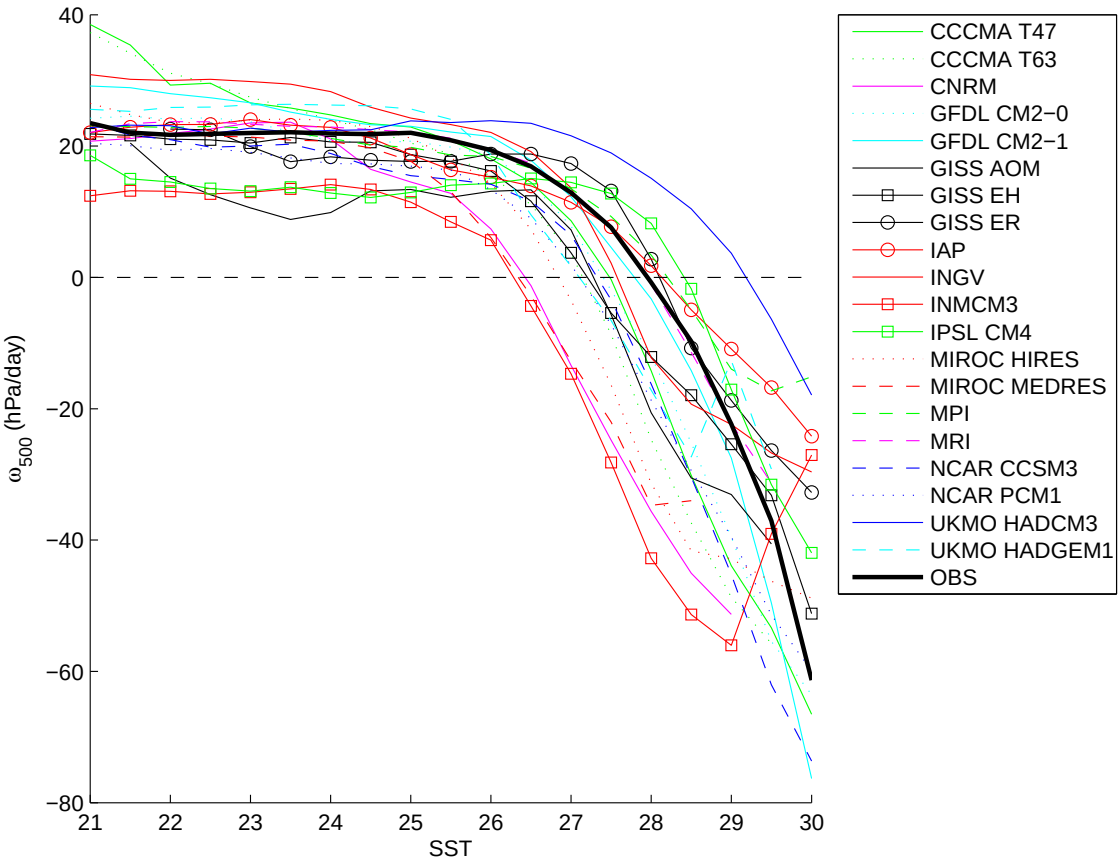

Fig. 14: Composite of ω_{500} (hPa/day) sorted by surface temperature regimes (^{o}C).

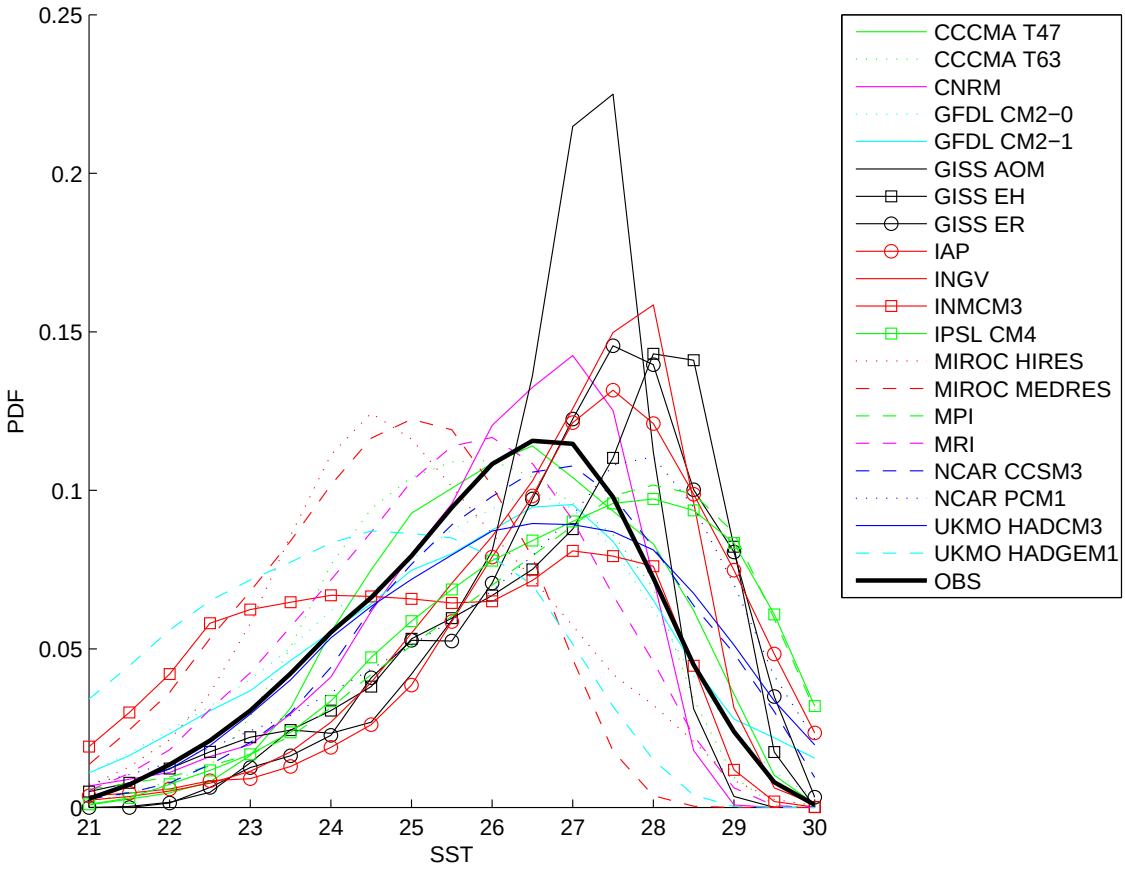

Fig. 15: Probability density function of sea surface temperature in the [150W-100W,20S-0] longitude-latitude range for AR4 models and observations (HadISST). Model PDFs are computed from monthly outputs from the 1960-2000 period of IPCC 20C3M simulations.

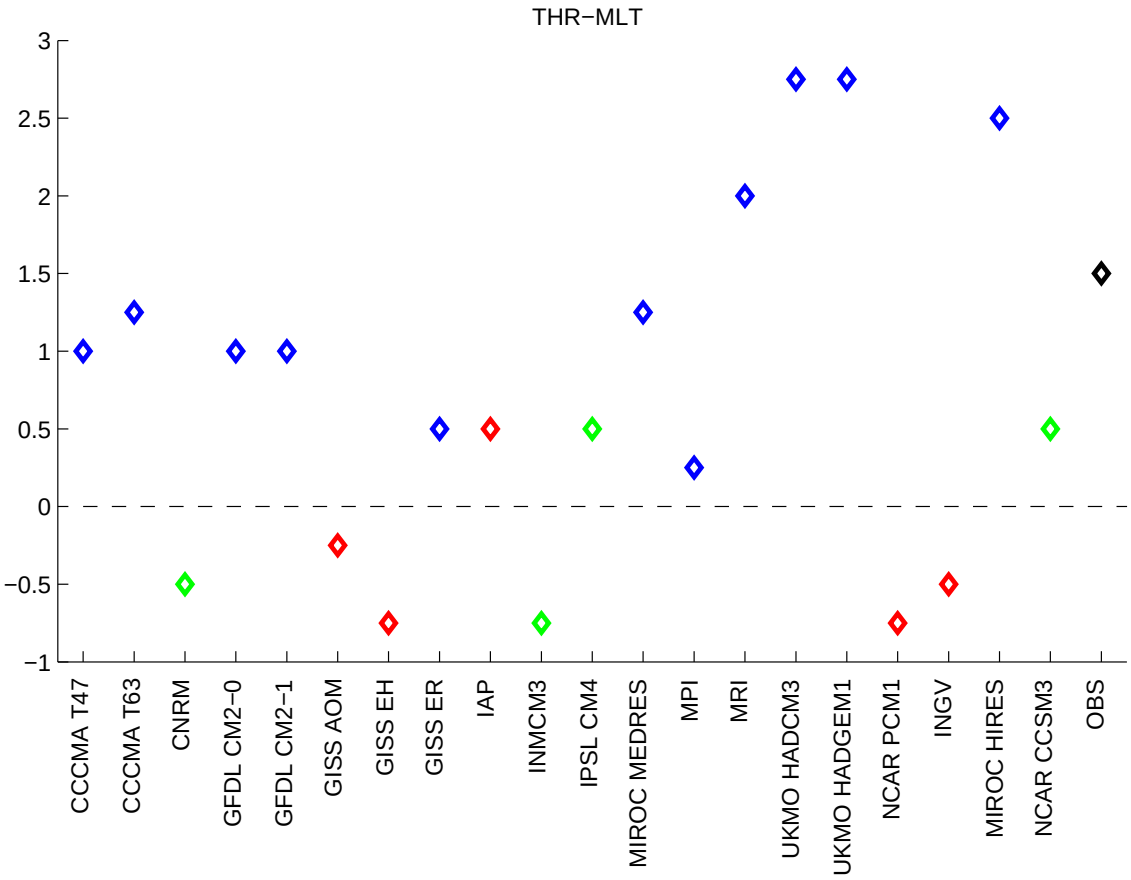

Fig. 16: Difference between THR and MLT temperature for models and observations (see text for details). Colors indicate whether the model falls within the SUB (blue), INT (red) or HYBRID (green) cluster. Black is used for observations.

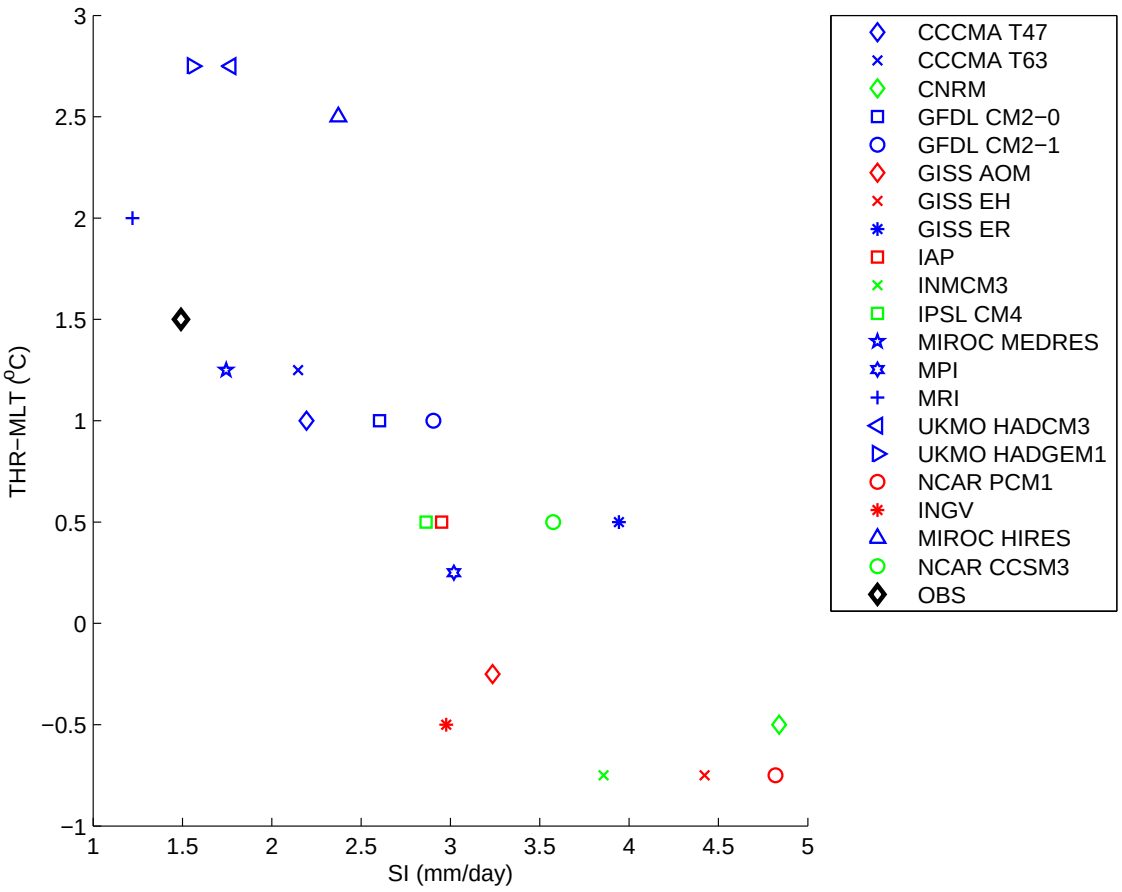

Fig. 17: Scatterplot of THR-MLT (^{o}C) and SI index (mm/day) for models and observations (see text for details). Colors indicate whether the model falls in the SUB (blue), INT (red) or HYBRID (green) cluster. Black is used for observations.